journal

J. Am. Ceram. Soc., 86 [2] 234–40 (2003)

Modeling of the Pressure Distribution in Three-Dimensional Porous Green Bodies during Binder Removal

Kai Feng* and Stephen J. Lombardo*

Department of Chemical Engineering, University of Missouri, Columbia, Missouri 65211

A model is developed to describe flow in porous media from the thermal decomposition of binder in three-dimensional bodies with anisotropic permeability. The model is able to describe the pressure within the body as a function of position, time, and temperature during the heating cycle. The results from numerical solution of the un-steady-state partial differential equation are compared to those obtained from an analytical solution to the steady-state equation. Under many conditions that are representative of binder removal, the analytical solution provides a reasonable representation of the numerical solution. A criterion is also developed to determine when the analytical solution is valid. Scaling relationships for the buildup of pressure in terms of the dimensions of the body, the rate of reaction, and the permeability are also derived.

I. Introduction

The removal of binder from green ceramic components by thermal methods involves a number of coupled kinetic and transport phenomena.[1,2] The difficulty in describing the kinetic phenomena arises because the rate of binder decomposition depends on the atmosphere and on catalytic effects between the solid phases and the organic phases.[2–6] Further complicating the description of binder degradation is that blends of organic phases are often used to aid in the processing of the green components, and each phase has different decomposition behavior. In spite of these difficulties, the kinetics of binder decomposition can be determined by first recording the weight loss of binder from thermogravimetric experiments and then using kinetic models to extract the preexponential factor and activation energy of the decomposition process. Although the kinetics can be accurately represented,[7,8] such rate expressions must be treated as apparent quantities because of the difficulty in treating the large number of individual reaction steps underlying the decomposition process.

The mass transport phenomena[1,2] that occur during binder removal include diffusion and capillary migration of low-viscosity components and the pressure-driven gas-phase flow of the binder decomposition products. The former mechanisms[9–16] are controlling during the initial stages of binder removal for green components highly loaded with organic phases, whereas the latter mechanism[6,8,16–20] is the more rapid transport process for bodies containing open porosity. Pressure-driven flow also occurs in bodies highly loaded with binder after interconnected porosity is created in the early stages of binder removal.

A number of efforts have been directed at solving the coupled kinetic and transport phenomena during binder removal,[6,11–20] and most of these have been restricted to one-dimensional (1-D) representations of the heat transfer and mass transfer equations. Even for the 1-D case, however, recourse to numerical solution of the coupled partial differential equations is required. The work of Tsai,[17] for example, treats the heat transfer and pressure-driven flow of binder decomposition products for bodies of 1-D infinite cylindrical shape. In addition to the numerical results, Tsai[17] was able to obtain an analytical solution for the 1-D pressure distribution within the body by invoking the pseudo-steady-state assumption and treating the temperature, and therefore the porosity, as uniform throughout the body. For bodies of radius 1 cm, the analytical solution agreed quite well with the numerical solution of the coupled heat and convective flow equations. For a larger body of 5 cm radius, however, the analytical solution proved much less satisfactory.

We have recently derived an analytical solution,[21,22] at the same level of approximation as Tsai used,[17] to the pressure-driven flow problem for 3-D bodies. The model can also treat anisotropic permeability within the body, because it has been observed in multilayer ceramic capacitors that flow is preferential parallel to the metal layers.[6] To obtain the analytical solution, we invoked the pseudo-steady-state assumption, which converts a 3-D un-steady-state partial differential equation into a 3-D Poisson's equation, the solution to which is an infinites series that converges rapidly. The advantage of the analytical solution is that the scaling relationships among the governing parameters are more readily apparent.

The focus of this work is to examine the impact of the pseudo-steady-state assumption on the accuracy of the model for describing the pressure distribution within green bodies. To do this, we have solved numerically the 3-D, partial differential equation for flow in porous media when a source term is present, and compared the results to those obtained from the analytical solution. The results obtained here indicate that for many problems of thermal binder removal, the analytical solution is satisfactory for describing the pressure field within the green body. We are also able to develop a criterion to assess under what conditions the analytical solution will be accurate. We then demonstrate some scaling relationships that can be obtained from the analytical solution.

II. Model

The governing equation for flow in a 3-D body (see Fig. 1) with porosity, ε, when a source term is present, is obtained from the continuity equation in terms of the molar gas density, ρ, and gas velocity, u_i ($i = x, y,$ or z), in each direction:[21,23]

$$-\left[\frac{\partial}{\partial x}(\rho u_x)+\frac{\partial}{\partial y}(\rho u_y)+\frac{\partial}{\partial z}(\rho u_z)\right]+\frac{r'}{M}=\frac{\partial(\rho\varepsilon)}{\partial t} \quad (1)$$

The rate of appearance of the products of binder degradation are denoted by r', and M is the molecular weight of the decomposition

G. W. Scherer—contributing editor

Manuscript No. 186874. Received June 26, 2002; approved November 22, 2002.
*Member, American Ceramic Society.

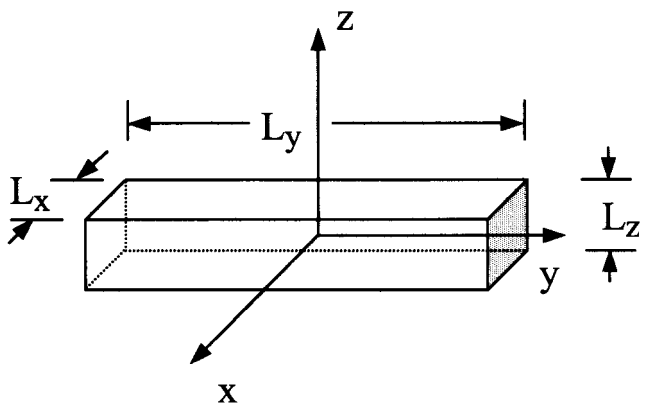

Fig. 1. Schematic of the green body defining the coordinate system and the length scales of the body.

products. The gas velocity in each direction in Eq. (1) can be represented by Darcy's law:

$$u_i = -\left(\frac{\kappa_i}{\mu}\right)\left(\frac{\partial P}{\partial i}\right) \tag{2}$$

where μ is the viscosity, P is the pressure, and κ_i is the permeability in each direction, each given by the Kozeny–Carmen equation:

$$\kappa_i = \frac{\varepsilon^3}{k_i(1-\varepsilon)^2 S^2} \tag{3}$$

where k_i is a constant that is related to the shape and tortuosity of the pores, and S is the surface area per unit volume of the green body. If the pore size is sufficiently small so that slip flow prevails,[17,24–27] then Eq. (2) can be corrected to account for this.

At low pressures, the gas is considered to be ideal and the molar gas density, ρ, is related to the pressure as

$$P = \rho RT \tag{4}$$

where R is the gas constant and T is the temperature. Combination of Eqs. (1), (2), and (4) leads to

$$\frac{\partial}{\partial x}\left[\rho\left(\frac{\kappa_x}{\mu}\right)\left(\frac{\partial(\rho RT)}{\partial x}\right)\right] + \frac{\partial}{\partial y}\left[\rho\left(\frac{\kappa_y}{\mu}\right)\left(\frac{\partial(\rho RT)}{\partial y}\right)\right] + \frac{\partial}{\partial z}\left[\rho\left(\frac{\kappa_z}{\mu}\right)\left(\frac{\partial(\rho RT)}{\partial z}\right)\right] + \frac{r'}{M} = \frac{\partial(\rho\varepsilon)}{\partial t} \tag{5}$$

Earlier work[6,8,9,17] has led to the following commonly used assumptions:

(1) The temperature distribution in the body is uniform at any point in time because of the slow heating rates and multiple hold periods used in binder removal cycles.

(2) The viscosity of the gas is constant during the heating cycle.

(3) The dimensional changes of the green body during binder removal are small and thus do not influence the pressure distribution.

We also define dimensionless stretched distances, gas density, and time, each denoted by an overbar, as[21,22]

$$\bar{x} = \frac{2x}{L_x} \tag{6a}$$

$$\bar{y} = \sqrt{\frac{\kappa_x}{\kappa_y}}\frac{2y}{L_x} \tag{6b}$$

$$\bar{z} = \sqrt{\frac{\kappa_x}{\kappa_z}}\frac{2z}{L_x} \tag{6c}$$

$$\bar{\rho} = \frac{\rho}{\rho_0} \tag{7}$$

$$\bar{t} = \frac{t}{\gamma} \tag{8}$$

where ρ_0 is the density of gas at ambient temperature T_0 and pressure P_0, and the dimensionless time is based on[20]

$$\gamma = \frac{\mu k_x S^2 L_x^2}{P_0} \tag{9}$$

Substitution of Eqs. (6) to (9) into Eq. (5) leads to

$$\frac{\partial}{\partial\bar{x}}\left[\bar{\rho}\left(\frac{\partial\bar{\rho}}{\partial\bar{x}}\right)\right] + \frac{\partial}{\partial\bar{y}}\left[\bar{\rho}\left(\frac{\partial\bar{\rho}}{\partial\bar{y}}\right)\right] + \frac{\partial}{\partial\bar{z}}\left[\bar{\rho}\left(\frac{\partial\bar{\rho}}{\partial\bar{z}}\right)\right] + \left(\frac{L_x^2}{4\rho_0^2\kappa_x}\right)\left(\frac{\mu}{RT}\right)\left(\frac{r'}{M}\right) = \left(\frac{L_x^2}{4\rho_0\kappa_x}\right)\left(\frac{\mu}{RT}\right)\left(\frac{1}{\gamma}\right)\left(\frac{\partial(\bar{\rho}\varepsilon)}{\partial\bar{t}}\right) \tag{10}$$

To complete the model description, we specify the reaction rate, r', as

$$r' = -\frac{\mathrm{d}(\rho_b\varepsilon_b)}{\mathrm{d}t} = A_0\exp\left(-\frac{E}{RT}\right)\rho_b\varepsilon_b \tag{11}$$

where ρ_b is the density of the binder, and ε_b is the volume fraction of binder, which is related to the volume fractions of porosity and solid, ε_s, as

$$\varepsilon = 1 - \varepsilon_s - \varepsilon_b \tag{12}$$

As the reaction proceeds and binder decomposes to gas-phase products, the evolution of the volume fraction of binder is given by

$$\varepsilon_b = \varepsilon_{b,0}\exp\left[-\int_0^t A_0\exp\left(-\frac{E}{RT}\right)\mathrm{d}t\right] \tag{13}$$

When Eqs. (11) to (13) are combined with Eq. (10) and rearranged, the following equation results:

$$\bar{\rho}\left(\frac{\partial^2\bar{\rho}}{\partial\bar{x}^2}\right) + \left(\frac{\partial\bar{\rho}}{\partial\bar{x}}\right)^2 + \bar{\rho}\left(\frac{\partial^2\bar{\rho}}{\partial\bar{y}^2}\right) + \left(\frac{\partial\bar{\rho}}{\partial\bar{y}}\right)^2 + \bar{\rho}\left(\frac{\partial^2\bar{\rho}}{\partial\bar{z}^2}\right) + \left(\frac{\partial\bar{\rho}}{\partial\bar{z}}\right)^2 + \frac{C}{2} = \left(\frac{C}{2}\right)\left(\frac{\rho_0 M}{\rho_b}\right)\bar{\rho} + \left(\frac{(1-\varepsilon)^2}{4\varepsilon^2}\right)\left(\frac{T_0}{T}\right)\left(\frac{\partial\bar{\rho}}{\partial\bar{t}}\right) \tag{14}$$

with

$$C = \left(\frac{L_x^2}{2\rho_0^2\kappa_x}\right)\left(\frac{\mu}{RT}\right)\left(\frac{r'}{M}\right) \tag{15}$$

Equation (14) is thus the governing nonlinear partial differential equation for flow in porous media when a source term is present.

The initial condition is $\bar{\rho} = 1$ at $\bar{t} = 0$ everywhere in the body, and the boundary condition at the edges of the body[21,22]

$$L = 1 \tag{16a}$$

$$W = \sqrt{\frac{\kappa_x}{\kappa_y}}\frac{L_y}{L_x} \tag{16b}$$

$$H = \sqrt{\frac{\kappa_x}{\kappa_z}}\frac{L_z}{L_x} \tag{16c}$$

is

$$\bar{\rho} = \frac{T_0}{T} \tag{17}$$

Once $\bar{\rho}$ has been determined, the pressure anywhere within the body can be obtained from

$$\frac{P}{P_0} = \bar{\rho}\left(\frac{T}{T_0}\right) \tag{18}$$

To obtain an analytical solution to Eq. (14), we can invoke the pseudo-steady-state assumption and use the transformation $\phi = \bar{\rho}^2$, which leads to

$$\frac{\partial^2\phi}{\partial\bar{x}^2} + \frac{\partial^2\phi}{\partial\bar{y}^2} + \frac{\partial^2\phi}{\partial\bar{z}^2} + C = 0 \tag{19}$$

Equation (19) is Poisson's equation for which the analytical solution is[21]

$$\phi = \left(\frac{T_0}{T}\right)^2 + \sum_{i=1,3,5,\ldots}\sum_{j=1,3,5,\ldots}\sum_{k=1,3,5,\ldots} A_{ijk} \times \cos\frac{i\pi\bar{x}}{2}\cos\frac{j\pi\bar{y}}{2W}\cos\frac{k\pi\bar{z}}{2H} \tag{20}$$

where

$$A_{ijk} = 8C\left(\frac{2}{\pi}\right)^5\left(\frac{1}{ijk\left[i^2 + \left(\frac{j}{W}\right)^2 + \left(\frac{k}{H}\right)^2\right]}\right)(-1)^{(i+j+k-3)/2} \tag{21}$$

The objective of this work is to compare the analytical solution given by Eq. (20) with the numerical solution of Eq. (14), which is obtained by a fully implicit backward finite-difference method.[28,29]

III. Results and Discussion

Before proceeding to the solution of Eq. (14) to describe the pressure distribution in porous bodies, the evaluation of the quantity C is of interest because this source term determines the magnitude of the pressure. With the exception of the terms for the reaction rate, r', body length, L_x, and permeability, κ_x, the other parameters in C span much smaller ranges for practical conditions of binder removal. With representative values in SI units of $\mu \approx 2 \times 10^{-5}$ Pa·s, $R = 8.314$ m^3·Pa/(mol·K), $T \approx 4 \times 10^2$ K, $M \approx 0.04$ kg/mol, $\rho_0 \approx 40$ mol/m^3, then $C \approx 4 \times 10^{-11} L_x^2 r'/\kappa_x$. For bodies fabricated from powders of 1 μm average particle size and 50% porosity, $\kappa_x \approx 2.5 \times 10^{-15}$ m^2 and thus $C \approx 10^4 L_x^2 r'$. For many ceramic bodies, the length is between 0.001 and 0.01 m and use of an intermediate value of $L_x = 0.01$ m leads to $C \approx r'$. The term for the rate of binder decomposition, r', is represented in an Arrhenius form which depends exponentially on temperature. Consequently, r' can span many orders of magnitude; for regions of interest when $P/P_0 > 1$, C must be greater than 1 as well, and thus r' must be greater than 1 kg/(m^3·s).

We first compare the numerical results for the time evolution of the pressure with the results from the analytical solution for the case of a constant source term C, which does not change with time. This will lead to a transient component of the pressure which will approach asymptotically the steady-state solution given by Eq. (20). Although this is not a physical situation representative of the binder burnout problem, where ε_b and r', and hence, C, change with time, this does allow for direct comparison of the numerical and analytical solutions and also serves as confirmation of the solution strategy. The values of the quantities used in the simulations are listed in Table I.

Figure 2 compares the results for the pressure at the center of the body, $P/P_0)_0$, as a function of time for different values of C. The geometry of the green body is a parallelepiped of dimensions $L = H = W = 1$, which can mean either a cube if the permeabilities are equal, or a rectangular shape with dimensions given by Eq. (16) once L_x and the permeabilities in each direction have been specified. For $C \leq 100$, which corresponds to pressure ratios in the center of the body of less than 5, a mesh of 11 nodes leads to good agreement between the long-time numerical solution of Eq. (14) and the analytical solution of Eq. (20). The transient component lasts approximately 0.5 unit of dimensionless time, which corresponds to 4.5 s from Eq. (9) if $L_x = 1$ cm. This implies that within this short time, the transient pressure field adjusts to the long-time solution.

For values of $C > 100$, higher pressures occur in the center of the body, and these are well above the values of 0.1–1 MPa that are believed to occur during binder burnout, although direct measurement of the internal pressure has never been reported. The transient component is shorter in dimensionless time, indicating that for a larger source term, i.e., a larger driving force, the flow field more quickly achieves the steady-state distribution. We also observe that with increasing value of C, more nodes are required for the two solutions to agree. In summary, the results in Fig. 2 indicate that because the transient component is short compared to the length of time of typical binder removal cycles, the flow field can be approximated by the steady-state pressure distribution. This latter statement will be quantified later in this work.

We next compare the numerical and analytical solutions for cases of binder removal where we now incorporate in the simulations a linear heating cycle $T = T_0 + \beta t$ with ramp rate, β, and account for binder decomposition with time and temperature as given by Eqs. (11) to (13). Figure 3 shows the pressure at the center of the body as a function of temperature for different ramp rates for a body of size $L_x = 2$ cm, $L_y = 4$ cm, and $L_z = 1$ cm. As the ramp rate is increased, the pressure at the center of the body increases, and the maximum occurs at progressively higher temperature. The analytical solution is also shown in Fig. 3, where very good agreement is obtained at low heating rates with a maximum discrepancy of about 5% at higher heating rates.

In Fig. 4, we show, in addition to $P/P_0)_0$, the evolution of the quantities ε_b, r', and C for $\beta = 1$°C/min. The trends in Fig. 4 indicate that the maximum in pressure does not coincide with the

Table I. Values of the Parameters Used in the Simulations

Symbol and description	Value and units
A_0, preexponential factor	8.5×10^{15} s^{-1}
E, activation energy	151.05 kJ/mol
T_0, initial temperature	300 K
P_0, initial ambient pressure	0.1 MPa
ε_s, solids fraction	0.5
$\varepsilon_{b,0}$, initial binder fraction	0.31
β, heating rate	0.01, 0.1, 1, 10, 15, 30°C/min
ρ_b, binder density	1000 kg/m^3
M, average molecular weight of gas products	0.044 kg/mol
μ, gas viscosity	0.025×10^{-3} Pa·s
S, specific surface area	6×10^6 m^{-1}
k_i, Kozeny–Carman parameter	5
L_x, L_y, L_z, body dimensions	2, 4, 1 cm; and 4, 8, 2 cm

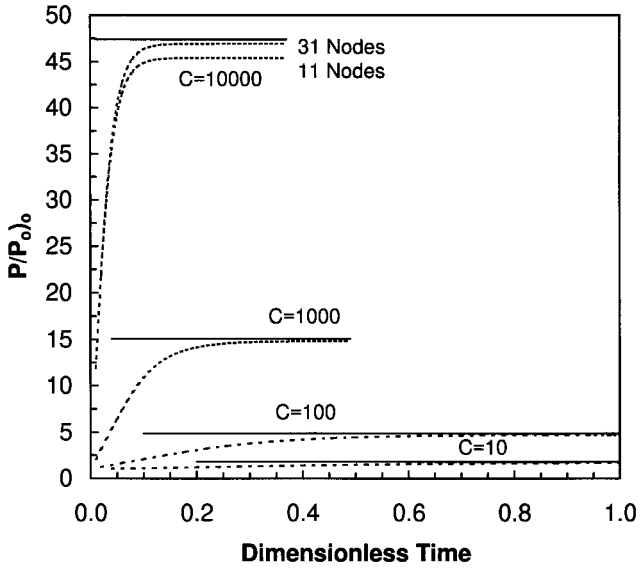

Fig. 2. Evolution of the pressure ratio at the center of the body as function of C for the initial condition $\bar{\rho} = 1$ at $\bar{t} = 0$. The size of the body is given by $L = W = H = 1$. Both the analytical solution (solid line) and the numerical solution (dashed line) are shown, the latter as a function of the number of nodes in each direction. For $C = 10$–100, the numerical solution for 11 nodes is shown. For $C = 1000$, the numerical solution for 21 nodes is shown. For $C = 10000$, the solutions for 11 and 31 nodes are used; with increasing number of nodes, the level of agreement is better.

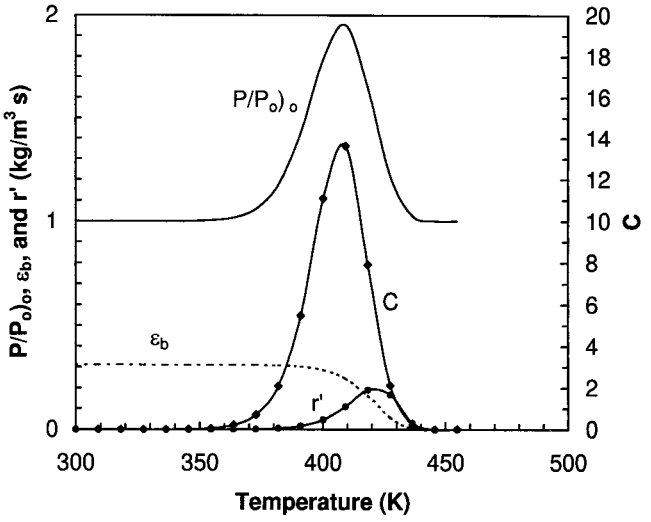

Fig. 4. Numerical solution for the pressure ratio at the center of the body, volume fraction of binder, reaction rate, and C as a function of temperature for a linear heating rate of 1°C/min. The dimensions of the body are $L_x = 2$ cm, $L_y = 4$ cm, and $L_z = 1$ cm.

maximum in the reaction rate but happens much earlier in the heating cycle when the body is nearly fully loaded with binder. The maximum in the pressure thus occurs when the reaction rate is relatively low, but the permeability is low as well, thus leading to a large resistance to flow. The maximum in the pressure does, however, coincide with the maximum in C. The same qualitative relationships in Fig. 4 among $P/P_0)_0$, ε_b, r', and C with temperature are also seen in the results (not shown here) for the other heating rates used in Fig. 3.

We next treat the case where the dimensions of the body are doubled so that $L_x = 4$ cm, $L_y = 8$ cm, and $L_z = 2$ cm. Figure 5 indicates that the magnitude of the pressure ratio at the center of the body increases as compared to the results for the same heating rate in Fig. 3. At the faster heating rates, the pressure at the center of the body is doubled as compared to the results in Fig. 3. The maxima in pressure, however, still occur at approximately the same temperatures as were observed for the smaller body in Fig. 3. When the results for the same heating rate in Figs. 3 and 5 are compared, the discrepancy between the numerical and analytical solutions is larger at the higher heating rates and for the body of larger size.

In Fig. 6, we show, in addition to $P/P_0)_0$, the evolution of other quantities ε_b, r', and C for $\beta = 15$°C/min. The trends in Fig. 6 are similar to what was observed in Fig. 4 in that the maximum in $P/P_0)_0$ does not occur at the same temperature as the maximum in the reaction rate but does coincide with the maximum in C.

The results in Figs. 2–6 show the pressure distribution at a single point in the body, namely in the center. We have also

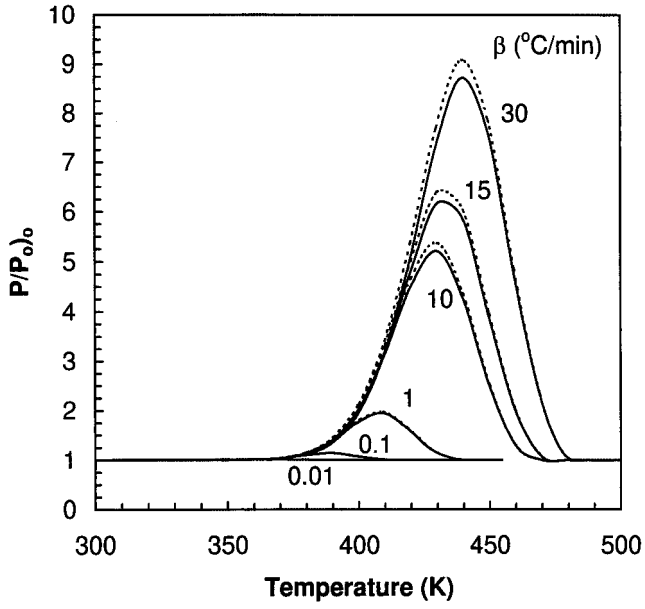

Fig. 3. Pressure ratio at the center of the body as a function of temperature for a linear heating rate. Both the analytical solution (dashed line) and the numerical solution (solid line) are shown. The dimensions of the body are $L_x = 2$ cm, $L_y = 4$ cm, and $L_z = 1$ cm.

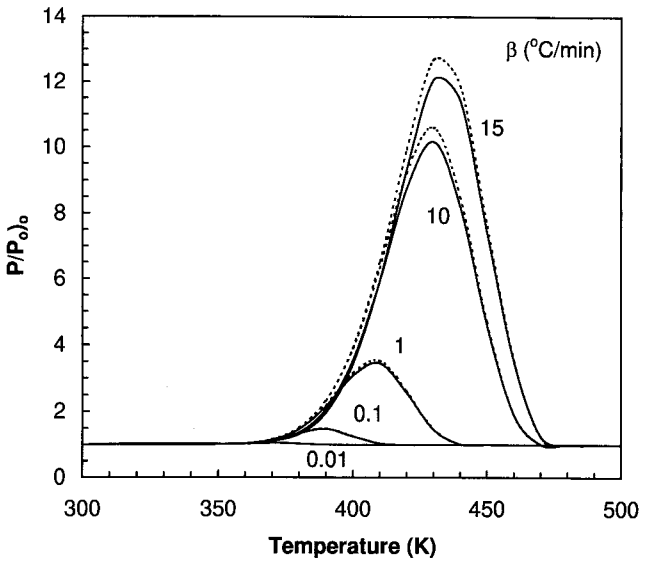

Fig. 5. Pressure ratio at the center of the body as a function of temperature for a linear heating rate. Both the analytical solution (dashed line) and the numerical solution (solid line) are shown. The dimensions of the body are $L_x = 4$ cm, $L_y = 8$ cm, and $L_z = 2$ cm.

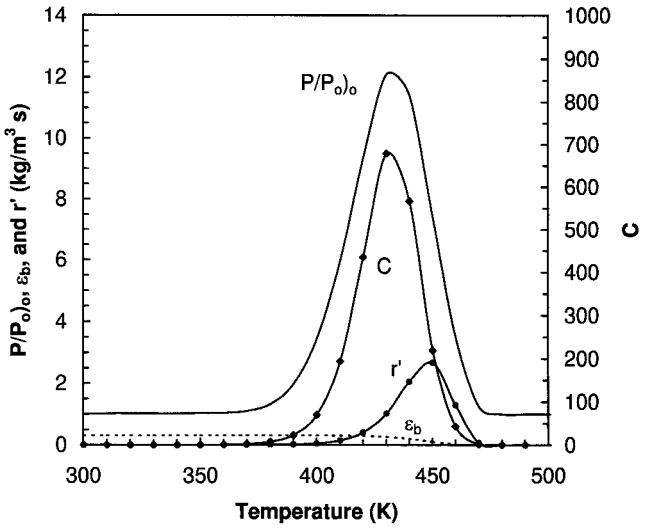

Fig. 6. Numerical solution for the pressure ratio at the center of the body, volume fraction of binder, reaction rate, and C as a function of temperature for a linear heating rate of 15°C/min. The dimensions of the body are L_x = 4 cm, L_y = 8 cm, and L_z = 2 cm.

determined the spatial distribution of pressure in the entire body, as determined from both the numerical and analytical solutions. Figure 7 contains the 2-D pressure profiles at T = 410 K in the heating cycle, which is when the maximum pressure ratio in the center of the body occurs. Figure 7 indicates that the pressure profiles are nonlinear throughout the body and decrease most rapidly as the edges of the body are approached. The trends in Fig. 7 further demonstrate that the analytical solution agrees well with the spatial distribution of pressure within the green body as determined from the numerical solution.

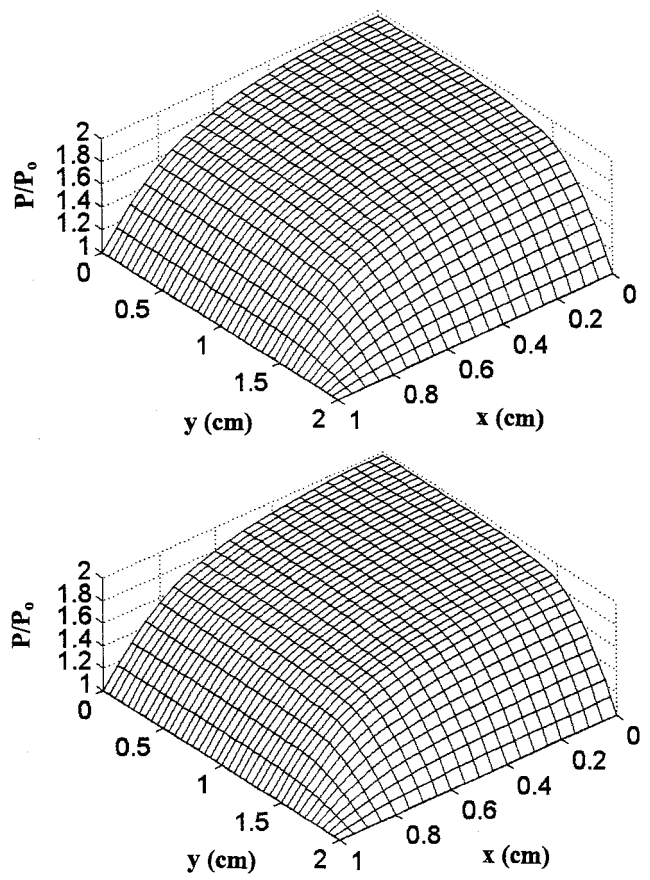

Fig. 7. Pressure profiles from the numerical solution (top panel) and analytical solution (bottom panel) for a heating rate of 1°C/min at T = 410 K and z = 0 cm. The dimensions of the body are L_x = 2 cm, L_y = 4 cm, and L_z = 1 cm.

The results in Figs. 2–6 show that the accuracy of the analytical solution, which is based on the pseudo-steady-state assumption, depends on both the quantity C and the heating rate, β. To determine the range of applicability of Eq. (20), it is thus necessary to evaluate when the right-hand side of Eq. (14) approaches zero:

$$\left(\frac{C}{2}\right)\left(\frac{\rho_0 M}{\rho_b}\right)\bar{\rho} + \left(\frac{(1-\varepsilon)^2}{4\varepsilon^2}\right)\left(\frac{T_0}{T}\right)\left(\frac{\partial\bar{\rho}}{\partial\bar{t}}\right) = \left(\frac{C}{2}\right)\left(\frac{\rho_0 M}{\rho_b}\right)\bar{\rho} + \left(\frac{(1-\varepsilon)^2}{4\varepsilon^2}\right)\left(\frac{T_0}{T}\right)\left(\frac{\partial\bar{\rho}}{\partial T}\right)\beta\gamma = 0 \quad (22)$$

for which the analytical solution is exact. We thus see that for Eq. (22) to be valid, the two terms containing C, β, and γ must add to a small quantity.

To proceed further, we set $\bar{\rho}$ = 10 and linearize the partial derivative with $\Delta\bar{\rho}$ = 10 and $\Delta\bar{t} = \Delta T/\beta\gamma$. This is equivalent to assuming that the pressure ratio varies linearly by a factor of 10 over the temperature range of interest. By substituting these values along with those from Table I, and setting ε = 0.3 and $T/T_0 \approx 1$, we obtain

$$10^{-2}\left(\frac{C}{2}\right) + 2\beta = 0 \quad (23)$$

The two terms in Eq. (23) are small if $C << 100$ and $\beta << 0.5$°C/s = 30°C/min. When these two criteria are met, the analytical solution will provide a reasonable representation of the numerical solution. The results in Figs. 3–6 for low heating rates all come close to satisfying both criteria; when the error is largest, both C and β are large as well. The form of Eq. (22), which contains a partial derivative with time, also indicates that in the early stages of the heating cycle, when the derivative is positive, the error should be larger than for later in the cycle, when the derivative is negative. This behavior is evident in the curves in Figs. 3 and 5.

Equation (22) can also be used to assess the validity of the model for other cases of binder removal. For bodies highly loaded with binder where $\varepsilon \to 0$, for which pressure-driven flow will not be the dominant transport mechanism, the term in Eq. (22) containing ε will be large, and thus the analytical solution would not be valid until additional porosity is created by another mechanism, such as leaching, diffusion, or evaporation. Equation (22) can thus be used to determine at what value of ε the analytical solution is valid.

The usefulness of the analytical solution can be extended by considering its form, which is an infinite series that converges rapidly.[21] Table II indicates the converged solution for many terms in the sum and for only the leading term in the series, i.e., $i = j = k = 1$ in Eqs. (20) and (21). For a fixed size of body, the error between the converged solution and the 1-term solution increases with increasing C and is also largest for bodies with 1 or more

Table II. Pressure Ratio at the Center of the Body from the Many Term Analytical Solution and the Error as Compared to When Only the Leading-Term Analytical Solution Is Used

L =	1	1	1	1	1	1	1	1
W =	1	1	1	10	1	1	1	10
H =	0.1	1	10	10	0.1	1	10	10
C	P/P$_0$)$_0$	P/P$_0$)$_0$	P/P$_0$)$_0$	P/P$_0$)$_0$	% error	% error	% error	% error
1	1.00	1.11	1.14	1.22	0.16	2.18	4.70	10.4
10	1.02	1.80	1.98	2.44	1.54	8.01	14.8	24.4
100	1.22	4.84	5.49	7.10	10.4	10.9	18.8	28.3
1000	2.44	15.0	17.1	22.3	24.4	11.3	19.3	28.8

lengths significantly different than L_x. In light of the difficulty in accurately specifying kinetic and permeability parameters, and the fact that the 1-term analytical solution is qualitatively in accord with the numerical solution, we can use the 1-term solution to develop scaling relationships.

The scaling relationships can be developed by evaluating the analytical solution at the center of the body where $\bar{x} = \bar{y} = \bar{z} = 0$ with only the leading term in the solution and C replaced by Eq. (15):

$$\left(\frac{P}{P_0}\right)_0 \approx \left[1 + 0.8365\left(\frac{L_x^2}{2\rho_0^2\kappa_x}\right)\left(\frac{\mu}{R}\right)\left(\frac{r'}{M}\right)\left(\frac{T}{T_0^2}\right) \times \left(\frac{W^2H^2}{W^2H^2 + W^2 + H^2}\right)\right]^{1/2} \tag{24}$$

When the buildup of pressure is large, which occurs when C is large, we obtain that $(P/P_0)_0$ is proportional to $(A_{111})^{1/2}$ and thus to all the terms appearing therein, as indicated in Eq. (24). To develop further scaling relationships, Eq. (24) can be simplified by incorporating Eq. (16) and then treating the case of equal permeability in all directions:

$$\left(\frac{P}{P_0}\right)_0 \propto \left[0.8365\left(\frac{1}{2\rho_0^2\kappa_x}\right)\left(\frac{\mu}{R}\right)\left(\frac{r'}{M}\right)\left(\frac{T}{T_0^2}\right) \times \left(\frac{L_x^2L_y^2L_z^2}{L_x^2L_y^2 + L_x^2L_z^2 + L_y^2L_z^2}\right)\right]^{1/2} \tag{25}$$

which is valid for large C.

A number of limiting cases can be examined. If all of the dimensions of the body are increased by the same factor, G, then $(P/P_0)_0 \propto G$, which is the behavior observed in Figs. 3 and 5 where the pressure ratio at the center of the body is doubled for a twofold increase in the dimensions of the body. As a subcase, if all of the dimensions of the body are nearly equivalent ($L_x \approx L_y \approx L_z$), then $(P/P_0)_0 \propto L_i$ where L_i is any one of the (equivalent) lengths of the body. Thus, the pressure ratio scales linearly with the dimension of the cubic body, or equivalently, scales with the cube root of the volume.

If one dimension is much smaller than the other two ($L_x << L_y$, L_z), then $(P/P_0)_0 \propto L_x$ and the pressure ratio scales with the smallest dimension, or in other words, the smallest length scale is the controlling resistance for the buildup of pressure. This case corresponds to, for example, large sections of thin tapes, where the thickness of the tape is the controlling resistance.

If one dimension is much larger than the other two ($L_x >> L_y$, L_z), then $(P/P_0)_0 \propto [L_y^2L_z^2/(L_y^2 + L_z^2)]^{1/2}$ and the pressure ratio is independent of the largest dimension. This corresponds to, for example, the geometry of high-aspect-ratio beams.

The full analytical solution can also be used to determine the temperature at which the maximum in pressure occurs, but this requires summation (Eq. (20)) and integration (Eq. (13)). Alternatively, the first-term analytical solution can be differentiated with respect to temperature to estimate the temperature at which the maximum occurs; this requires solution of a nonlinear equation containing integrals from Eq. (13). We note, however, that to perform this differentiation, the only quantities in Eq. (25) changing with temperature, and thus time, appear as $r'T/\kappa_x$. We can thus approximate[29] the exponential in Eq. (13), and then derive an algebraic equation for ε_b at any temperature as

$$\ln\frac{\varepsilon_{b,0}}{\varepsilon_b} = \frac{A_0}{\beta}\left[\frac{\left(\frac{RT^2}{E}\right)\exp\left(-\frac{E}{RT}\right)}{1 + \frac{2RT}{E}} - \frac{\left(\frac{RT_0^2}{E}\right)\exp\left(-\frac{E}{RT_0}\right)}{1 + \frac{2RT_0}{E}}\right] \tag{26}$$

Equation (26) can then be used with Eq. (25) to graphically determine the temperature at which the maximum in the pressure ratio occurs. Temperatures determined in this manner agree within ± 3°C with those predicted from the numerical results reported in Figs. 3 and 5.

In summary, the analytical solution given by Eq. (20) can be considered accurate when the assumptions in the model are realized, and the criterion given by Eq. (22) is approximately satisfied. The most important of the assumptions is that the temperature is uniform across the body and that the heating rate is low. Because most binder removal cycles, which contain slow ramps with multiple holds, are developed to avoid failure of the body, these conditions may be met in practice. When these conditions are not met, then the heat transfer model[6,16,17,20] must be solved numerically as well, in conjunction with Eq. (14).

Although this work focuses on the pressure distribution within green bodies, the stress is ultimately what causes failure of the body. In the formulation of the stress problem,[22] however, the pressure gradient within the body, which can be treated as an internal body force, appears in the governing mechanics equations. When the internal pressure distribution can be represented by an analytical function, then the stress problem can be solved using commercially available finite-element programs for 3-D bodies. The analytical solution for the pressure presented in this work was originally derived for this specific purpose.

IV. Conclusions

In this work, we have treated the case of binder removal from 3-D bodies where the permeability may be anisotropic. The rate of binder degradation is modeled as an activated rate process; after degradation, the gas-phase decomposition products flow out of the body under the influence of a pressure field. We have compared the pressure profiles, as calculated by numerical methods from the un-steady-state partial differential equation, with those predicted by an analytical solution. In general, for the range of heating rates typically used in binder removal cycles, the level of agreement is quite good, with results typically within 5% of the numerical simulation. A criterion has also been developed to indicate when the analytical solution is valid. In light of the difficulty in accurately specifying reaction kinetics and permeabilities of porous media, the analytical solution is useful for obtaining pressure distributions and scaling relationships for binder removal from 3-D green bodies.

References

[1]R. M. German, "Theory of Thermal Debinding," *Int. J. Powder Metall.*, **23**, 237–45 (1987).

[2]J. A. Lewis, "Binder Removal From Ceramics," *Annu. Rev. Mater. Sci.*, **27**, 147–73 (1997).

[3]H. H. G. Jellinek, "Degradation and Depolymerization Kinetics"; pp. 1–37 in *Aspects of Degradation and Stabilization of Polymers*. Edited by H. H. G. Jellinek. Elsevier, New York, 1978.

[4]S. Masai, P. D. Calvert, W. E. Rhine, and H. K. Bowen, "Effect of Oxides on Binder Burnout During Ceramics Processing," *J. Am. Ceram. Soc.*, **24**, 1907 (1989).

[5]A. Nair and R. White, "Effects of Inorganic Oxides on Polymer Binder Burnout: I, Poly(vinyl butyral)," *J. Appl. Polym. Sci.*, **60**, 1901–909 (1996).

[6]L. C.-K. Liau, B. Peters, D. S. Krueger, A. Gordon, D. S. Viswanath, and S. J. Lombardo, "Role of Length Scale on Pressure Increase and Yield of Poly(vinyl butyral)–Barium Titanate–Platinum Multilayer Ceramic Capacitors During Binder Burnout," *J. Am. Ceram. Soc.*, **83**, 2645–53 (2000).

[7]P. Calvert and M. Cima, "Theoretical Models for Binder Burnout," *J. Am. Ceram. Soc.*, **73**, 575–79 (1990).

[8]R. V. Shende and S. J. Lombardo, "Determination of Binder Decomposition Kinetics for Specifying Heating Parameters in Binder Burnout Cycles," *J. Am. Ceram. Soc.*, **85**, 780–86 (2002).

[9]M. R. Barone and J. C. Ulicny, "Liquid-Phase Transport During Removal of Organic Binders in Injection-Molded Ceramics," *J. Am. Ceram. Soc.*, **73**, 3323–33 (1990).

[10]M. J. Cima, J. A. Lewis, and A. D. Devoe, "Binder Distribution in Ceramic Greenware During Thermolysis," *J. Am. Ceram. Soc.*, **72**, 1192–99 (1989).

[11]J. R. G. Evans, M. J. Edirisinghe, J. K. Wright, and J. Crank, "On the Removal of Organic Vehicle from Moulded Ceramic Bodies," *Proc. R. Soc. London, A*, **432**, 321 (1991).

[12]S. A. Matar, M. J. Edirisinghe, J. R. G. Evans, and E. H. Twizell, "Effect of Porosity Development on the Removal of Organic Vehicle from Ceramic or Metal Moldings," *J. Mater. Res.*, **8**, 617–25 (1993).

[13]S. A. Matar, M. J. Edirisinghe, J. R. G. Evans, and E. H. Twizell, "Diffusion of Degradation Products in Ceramic Moldings during Thermal Pyrolysis: Effect of Geometry," *J. Am. Ceram. Soc.*, **79**, 749–55 (1996).

[14]T. S. Shivashankar and R. M. German, "Effective Length Scale for Predicting Solvent-Debinding Times of Components Produced by Powder Injection Molding," *J. Am. Ceram. Soc.*, **82**, 1146–52 (1990).

[15]J. A. Lewis, M. A. Galler, and D. P. Betz, "Computer Simulation of Binder Removal from 2-D and 3-D Model Particulate Bodies," *J. Am. Ceram. Soc.*, **79**, 1377–88 (1996).

[16]G. Y. Stangle, and I. A. Aksay, "Simultaneous Momentum, Heat and Mass Transfer with Chemical Reaction in a Disordered Porous Medium: Application to Binder Removal from a Ceramic Green Body," *Chem. Eng. Sci.*, **45**, 1719–31 (1990).

[17]D.-S. Tsai, "Pressure Buildup and Internal Stresses During Binder Burnout: Numerical Analysis," *AIChE J.*, **37**, 547–54 (1991).

[18]S. A. Matar, M. J. Edirisinghe, J. R. G. Evans, E. H. Twizell, and J. H. Song, "Modeling the Removal of Organic Vehicle from Ceramic or Metal Moldings: The Effect of Gas Permeation on the Incidence of Defects," *J. Mater. Sci.*, **30**, 3805–10 (1995).

[19]J. H. Song, M. J. Edirisinghe, J. R. G. Evans, and E. H. Twizell, "Modeling the Effect of Gas Transport on the Formation of Defects during Thermolysis of Powder Moldings," *J. Mater. Res.*, **11**, 830–40 (1996).

[20]A. C. West and S. J. Lombardo, "The Role of Thermal and Transport Properties on the Binder Burnout of Injection Molded Ceramic Components," *Chem. Eng. J.*, **71**, 243–52 (1998).

[21]S. J. Lombardo and Z. C. Feng, "Pressure Distribution during Binder Burnout in Three-Dimensional Porous Ceramic Bodies with Anisotropic Permeability," *J. Mater. Res.*, **17**, 1434–40 (2002).

[22]Z. C. Feng, B. He, and S. J. Lombardo, "Stress Distribution in Porous Ceramic Bodies During Binder Burnout," *J. Appl. Mech.*, **69**, 497–501 (2002).

[23]M. E. Harr, *Mechanics of Particulate Media*. McGraw-Hill, New York, 1997.

[24]L. J. Klinkenberg, "The Permeability of Porous Media to Liquids and Gases," *Drill. Prod. Pract., API*, 200–13 (1941).

[25]G. P. Brown, A. DiNardo, G. K. Cheng, and T. K. Sherwood, "The Flow of Gases in Pipes at Low Pressures," *J. Appl. Phys.*, **17**, 802–13 (1946).

[26]N. Wakao, S. Otani, and J. M. Smith, "Significance of Pressure Gradients in Porous Materials: Part I, Diffusion and Flow in Fine Capillaries," *AIChE J.*, **11**, 435–39 (1965).

[27]S. Otani, N. Wakao, and J. M. Smith, "Significance of Pressure Gradients in Porous Materials: Part II, Diffusion and Flow in Porous Catalysts," *AIChE J.*, **11**, 439 (1965).

[28]W. F. Ames, *Numerical Methods for Partial Differential Equations*, 3rd Ed. Academic Press, New York, 1992.

[29]T. V. Lee and S. R. Beck, "A New Integral Approximation Formula for Kinetic Analysis of Nonisothermal TGA Data," *AIChE J.*, **30**, 517–19 (1984). □